Effect of the symmetry energy on the secondary component of GW190814 as a neutron star

Xuhao Wu [1,2,*] Shishao Bao,[3,†] Hong Shen [4,‡] and Renxin Xu[1,2,§]

[1]*School of Physics, Peking University, Beijing 100871, China*

[2]*Kavli Institute for Astronomy and Astrophysics, Peking University, Beijing 100871, China*

[3]*School of Physics and Information Engineering, Shanxi Normal University, Linfen 041004, China*

[4]*School of Physics, Nankai University, Tianjin 300071, China*

(Received 15 January 2021; revised 4 May 2021; accepted 24 June 2021; published 13 July 2021)

The secondary component of GW190814 with a mass of 2.50–2.67 $M_\odot$ may be the lightest black hole or the heaviest neutron star ever observed in a binary compact object system. To explore the possible equation of state (EOS), which can support such a massive neutron star, we apply the relativistic mean-field model with a density-dependent isovector coupling constant to describe the neutron-star matter. The acceptable EOS should satisfy some constraints: the EOS model can provide a satisfactory description of the nuclei; the maximum mass $M_{\rm TOV}$ is above 2.6 $M_\odot$; the tidal deformability of a canonical 1.4 $M_\odot$ neutron star $\Lambda_{1.4}$ should lie in the constrained range from GW170817. In this paper, we find that nuclear symmetry energy and its density dependence play a crucial role in determining the EOS of neutron-star matter. The constraints from the mass of 2.6 $M_\odot$ and the tidal deformability $\Lambda_{1.4} = 616^{+273}_{-158}$ (based on the assumption that GW190814 is a NS-BH binary) can be satisfied for the slope of symmetry energy $L \leqslant 50$ MeV. Even including the constraint $\Lambda_{1.4} = 190^{+390}_{-120}$ from GW170817 which suppresses the EOS stiffness at low density, the possibility that the secondary component of GW190814 is a massive neutron star cannot be excluded in this study.

DOI: 10.1103/PhysRevC.104.015802

I. INTRODUCTION

The first direct detection of gravitational waves from GW150914 [1], the merger of a pair of black holes, launched a new era of gravitational-wave astronomy. Two years later, the binary neutron star merger event GW170817 [2], which was observed by the LIGO and Virgo detectors, produced a detectable electromagnetic signal and marked a significant breakthrough for multimessenger astronomy. After that, another binary neutron star merger event GW190425 was detected in April of 2019 [3]. Several months after GW190425, in the third observing run of Advanced LIGO and Advanced Virgo [4], a gravitational wave signal GW190814 was discovered from a compact binary coalescence involving a 22.2–24.3 $M_\odot$ black hole and a compact object of 2.50–2.67 $M_\odot$. Since no measurable tidal signature was detected from the gravitational waveform and no electromagnetic counterpart of GW190814 was confirmed, the secondary component of GW190814 could be either the heaviest neutron star or the lightest black hole ever discovered [4]. Although the highest measured mass of radio pulsars is around 2.14 $M_\odot$ [5], the equation of state (EOS) should be very stiff at high density if the maximum neutron-star mass is assumed to be $M_{\rm TOV} > 2.3\,M_\odot$ [6].

It seems difficult to determine the nature of GW190814 by further analyzing the data, that many theoretical studies have been devoted to exploring various possibilities of the secondary component of GW190814. It has been reported in Ref. [4] that GW190814 has a highly unequal mass ratio of $0.112^{+0.008}_{-0.009}$ and unusual secondary mass of $2.59^{+0.08}_{-0.09}$ $M_\odot$, which lies in the mass gap between neutron stars and black holes. These two features make GW190814 rare to explore supernova explosion mechanism, canonical isolated binary evolution, and massive star evolution, which have been discussed in Refs. [7,8]. Bayesian analysis [9–11] gives distinguishing results that depend on the choice of EOS parametrization and the maximum mass threshold. For example, if the maximum mass limit of $M_{\rm TOV} < 2.3\,M_\odot$ suggested by Shibata *et al.* [12] is enforced, the probability of GW190814 to be a neutron star-black hole (NS-BH) merger will significantly reduced [9]. Similar results were also shown within a nuclear-physics-multimessenger astrophysics framework [13]. In Ref. [14] Nathanail *et al.* used a genetic algorithm to sample the multidimensional space of parameters from GW170817 gravitational-wave and astronomical observations, and they concluded that the secondary in GW190814 was most likely a black hole at merger. On the other hand, if the low-mass object of GW190814 is a neutron star, it would provide strong constraints on EOS, in tension with those inferred from the GW170817 event. However, it is also possible that the secondary in GW190814 is a rapidly rotating neutron star [10,15–21]. With the inclusion of rotation effects, the maximum mass could be about 20% larger than $M_{\rm TOV}$ of a nonrotating neutron star [22,23], and as a result, the

*x.h.wu@pku.edu.cn

†bao_shishao@163.com

‡shennankai@gmail.com

§r.x.xu@pku.edu.cn

upper limit $M_{\rm TOV} < 2.3\ M_\odot$ inferred from the multimessenger observations of GW170817 [12] could be compatible with the secondary in GW190814 being a rapidly rotating neutron star [17,20]. Generally, the frequency required to support a 2.5 $M_\odot$ neutron star is very high, which is even higher than the maximum rotation frequency of 716 Hz observed from the fastest known pulsar, PSR J1748-2446ad [24], associated with a dimensionless spin of $0.25 \leqslant \chi \leqslant 0.65$ [25]. Therefore, the possibility of the secondary in GW190814 as a rapidly rotating neutron star cannot be ruled out. Another possibility to achieve high neutron-star masses has been discussed in modified gravity theories [26–28].

Even without the effects of modified gravity or fast rotation, the constraints from GW170817 [2,29] still allow the existence of stiff enough EOS to support 2.5 $M_\odot$ slowly rotating (or nonrotating) neutron stars [30–34]. For example, a Markov chain Monte Carlo approach was raised by Godzieba *et al.* [32] to generate phenomenological EOSs that could satisfy the astronomical constraints and support the GW190814 is a NS-BH system. Fattoyev *et al.* [33] proposed the BigApple parameter set in covariant energy density functional theory, which predicts the maximum neutron-star mass of 2.6 $M_\odot$ and can reproduce the observables of finite nuclei and NICER. The appearance of deconfined QCD matter in neutron stars may support massive neutron stars with $M_{\rm TOV} > 2.5\ M_\odot$ [34]. This view is also indirectly supported by the quarkyonic matter influence on the EOS [35]. Moreover, the possibility of GW190814 being a quark star–black hole system was discussed in Refs. [36–38].

To assess the nature of the secondary component of GW190814, the EOS at high density plays an essential role. It is well known that the EOS is crucial in determining the mass-radius relation of neutron stars. However, there are large uncertainties in the strong interaction at high density, and calculations of neutron-star matter are generally performed with effective interactions [39]. Especially, phenomenological mean-field models have been widely used for describing the EOS of neutron stars.

In this work, we use the relativistic mean-field (RMF) model to describe the neutron-star matter, in which nucleons interact via the exchange of various mesons. The RMF model parameters are typically determined by fitting some experimental data of finite nuclei or empirical saturation properties at the nuclear saturation density n_0, i.e., the binding energy per nucleon (E/A), the nuclear incompressibility (K), the symmetry energy (S), and the effective mass (m^*/m). The symmetry energy slope (L), which has an apparent effect on the neutron-star radius and the neutron-skin thickness of neutron-rich nuclei [40–42], is another important parameter that has been extensively studied in recent years [39,43–45]. However, its value is still very uncertain and cannot be well constrained from current observations. In order to explore the influence of symmetry energy slope, one may introduce density-dependent isovector couplings or add ω-ρ coupling term [46]. The two approaches are basically equivalent [47]. In this paper, we will use the RMF model with a density-dependent isovector coupling (referred to as the RMFL model following Ref. [48]). Through this way, the symmetry energy slope L can be tailored by adjusting an additional coefficient without affecting the other saturation properties, and remaining all parameters unchanged. In general, the low-density EOSs have similar energy-pressure curves, since they can be well constrained by experimental data of finite nuclei or saturation properties of nuclear matter. However, the high-density component of the EOS remains largely uncertain, which has to be constrained by neutron star observations.

Over the past decade, several massive neutron stars have been discovered, PSR J1614-2230 [49–51], PSR J0348+0432 [52], PSR J0740+6620 [5], and PSR J2215+5135 [53], which imposed a lower bound to the maximum mass of neutron stars ($M_{\rm TOV} > 2\ M_\odot$). Moreover, the binary neutron star merger event GW170817 provides new constraints on the tidal deformability of a canonical 1.4 $M_\odot$ neutron star, $\Lambda_{1.4} \leqslant 800$ reported in the discovery paper [2] and the updated value of $\Lambda_{1.4} = 190^{+390}_{-120}$ in Ref. [54]. The radius of a 1.4 $M_\odot$ neutron star $R_{1.4}$ could be constrained to be $R_{1.4} \leqslant 13.6$ km within different models [29,55]. Besides, based on NASA's Neutron Star Interior Composition Explorer (NICER) data set, an estimation for the mass-radius relation becomes possible by using x-ray pulse-profile modeling [56]. Through this way, the mass and radius of PSR J0030+0451 were reported as ($1.44^{+0.15}_{-0.14}\ M_\odot$, $13.02^{+1.24}_{-1.06}$ km) [57] or ($1.34^{+0.15}_{-0.16}\ M_\odot$, $12.71^{+1.14}_{-1.19}$ km) [58] by different groups. Among these observational properties, neutron-star mass and tidal deformability are dynamical and model-independent measurements that provide strong constraints, while the radius may have different results from various models. It is believed that the binary neutron star merger event GW170817 may eventually become a black hole. Based on this assumption, upper bounds on $M_{\rm TOV}$ supported by the EOS are placed to be $M_{\rm TOV} \approx 2.3\ M_\odot$ [12,59–62]. But without this assumption on the remnant, larger $M_{\rm TOV}$ could be achieved [62]. Besides, $M_{\rm TOV} > 2.3\ M_\odot$ cannot be ruled out from the views of astrophysics and microphysics.

Besides the constraints from astrophysical observations, nuclear matter calculations with realistic nucleon-nucleon interaction in chiral effective field theory [63–67], which links baryonic few-body forces to QCD, could provide valuable constraints with uncertainty estimates on the EOS, symmetry energy, and its slope. For example, the calculation of Holt and Kaiser with a specific chiral interaction gives $20 < L < 65$ MeV [66], which is consistent with the constraint $40 < L < 60$ MeV inferred from the experimental data [45]. Oertel *et al.* [39] summarized a sufficient number of constraints from various studies and they found the most probable value for the symmetry energy slope is $L = 58.7 \pm 28.1$ MeV. In addition, the newly announced PREX-II measurement reported a value of 0.283 ± 0.071 fm [68] for the neutron-skin thickness of ^{208}Pb, implying a slope parameter $L = 106 \pm 37$ MeV [69], which is larger than most values extracted from various experimental and theoretical analyses [39]. It is worth noting that the large slope parameter L from PREX-II does not directly imply a large radius for a neutron star in the canonical mass range. By combining astrophysical data with PREX-II and chiral effective field theory constraints, a nonparametric analysis leads to $L = 58 \pm 19$ MeV [70].

In this paper, we aim to use the RMFL model with the NL3 parametrization to generate a series of density-dependent

isovector coupling parameter sets (referred to as NL3L) with different symmetry energy slope L. The original NL3 parametrization [71] was proposed by fitting experimental data of ten selected nuclei, including the binding energies, charge radii, and neutron radii, while some nuclear matter properties were also considered in the fitting procedure. As a result, the NL3 model could provide a satisfactory description for both spherical and deformed nuclei throughout the nuclear chart, and its predicted saturation properties are consistent with empirical values. Furthermore, the NL3 model has been widely used in astrophysical studies, such as neutron star and supernova EOS [39]. In the present work, we extend the NL3 model by using a density-dependent isovector coupling, so that the symmetry energy slope L can be adjusted in the range considered. The generated NL3L models have the same saturation properties as the original NL3 except with different values of L. Since the ground-state properties of finite nuclei are insensitive to the slope parameter L, the NL3L models are expected to provide similar results of finite nuclei as the original NL3. However, different L values in NL3L may have a significant influence on neutron-star properties. Using the NL3L parameter sets, we examine the role of symmetry energy slope L in neutron-star matter EOS and properties of neutron stars. It is believed that a smaller L corresponds to a softer EOS in the density range from n_0 to ≈ 0.3 fm^{-3}, which mainly affects the radius and tidal deformability of neutron star with $M < 1.5\,M_\odot$. It is noteworthy that the coupling constants in the RMF approach are not observables, which are usually determined by fitting experimental results of finite nuclei as in the case of the NL3 parametrization. With the coupling constants constrained around saturation density, the extrapolation to high-density region would yield model-dependent predictions for neutron stars.

It is crucial to discuss the theoretical uncertainty in order to assess the reliability of extrapolations [72]. In recent years, theoretical uncertainty estimates have been developed in various frameworks [73–80]. The chiral effective field theory can provide uncertainty estimates by performing order-by-order calculations in the chiral expansion [66], but the reliability of such estimates is still a subject of ongoing research. Unfortunately, most of the successful RMF parametrizations, such as NL3, have not considered any uncertainty when they were calibrated from selected experimental data of finite nuclei. A newly proposed parametrization FSUGold2 [74] provided quantified statistical uncertainties for various physical observables by using a Gaussian approximation to the likelihood function. The uncertainty estimates obtained from the FSUGold2 parametrization may be considered as typical values, which can help to understand theoretical uncertainties in the RMF models. In the calibration procedure of FSUGold2 [74], a maximum neutron-star mass $M_{\rm TOV} = 2.1\,M_\odot$ was incorporated into the fitting scheme in addition to experimental data of finite nuclei. After the optimization, the FSUGold2 parametrization yielded the predictions with uncertainty estimates for neutron stars as $M_{\rm TOV} = 2.07 \pm 0.02\,M_\odot$ and $R_{1.4} = 14.42 \pm 0.26$ km. However, when the maximum neutron-star mass was removed from the calibration, the uncertainties of $M_{\rm TOV}$ and $R_{1.4}$ increased to about $0.15\,M_\odot$ and 0.78 km, respectively. It is reasonable to consider that uncertainty estimates using the NL3 parametrization should have the same order of magnitude, since similar observables of finite nuclei were adopted in the fitting procedures of NL3 and FSUGold2 [74]. In this type of model, the isoscalar saturation properties can be well determined with small theoretical errors, but the isovector part, especially the symmetry energy slope L, remains large uncertainties due to the lack of well-measured isovector observables in the fit. In the present work, we investigate the influence of uncertain slope parameter L on the EOS and properties of neutron stars by using the generated NL3L models covering an acceptable range of L. Qualitatively, the theoretical errors in NL3L would be of the same order as the original NL3 model due to their similarities discussed above. Furthermore, except the statistical errors analyzed in Ref. [74], there are various systematic errors in the RMF models, which are very difficult to estimate quantitatively [75]. One may assess systematic uncertainties of the RMF models by making comparisons among different parametrizations [79]. The present calculations using the NL3L parameter sets would be helpful to understand the uncertainty caused by the slope parameter L.

In general, the presence of exotic degrees of freedom, like hyperons and quarks, tends to soften the EOS at high densities and reduce the maximum mass of neutron stars [81–83]. However, this effect can be suppressed by considering the additional repulsion for hyperons (or quarks). Furthermore, the crossover hadron-quark phase transition may provide a stiffer quarkyonic core in neutron stars. The possibility of the secondary in GW190814 as a massive neutron star with exotic degrees of freedom has been discussed in Refs. [15,19,21,31]. For simplicity, we do not include non-nucleonic degrees of freedom in the present work. We aim to investigate the symmetry energy effect on the properties of massive neutron stars and explore the possibility of the secondary component of GW190814 as a neutron star.

This article is organized as follows. In Sec. II, we briefly introduce the RMFL model for neutron-star matter. In Sec. III, we show the numerical results of neutron-star properties and compare with constraints from astronomical observations. Section IV is devoted to a summary.

II. RMF WITH A DENSITY-DEPENDENT ISOVECTOR COUPLING CONSTANT

We adopt the RMFL model to describe the neutron-star matter, in which the isovector coupling constant is taken to be density dependent as in the density-dependent RMF

TABLE I. Parameters in the NL3 model. The masses are given in MeV.

Model	M	m_σ	m_ω	m_ρ	g_σ	g_ω	$g_\rho(n_0)$	g_2 (fm^{-1})	g_3
NL3	939.000	508.194	782.501	763.000	10.217	12.868	8.948	−10.431	−28.885

TABLE II. Nuclear matter saturation properties obtained in the NL3 model. All quantities are given in MeV, except the dimensionless effective mass m^*/m, and the saturation density n_0, given in fm^{-3}.

Model	n_0	E/A	K	S	L	m^*/m
NL3	0.148	−16.24	272.3	37.4	118.5	0.594

(DDRMF) approach. We use the Lagrangian given as

$$\begin{aligned}\mathcal{L}_{\rm RMFL} = &\sum_{i=p,n}\bar{\psi}_i\Big\{i\gamma_\mu\partial^\mu - (M+g_\sigma\sigma)\\ &-\gamma_\mu\Big[g_\omega\omega^\mu + \frac{g_\rho}{2}\tau_a\rho^{a\mu}\Big]\Big\}\psi_i\\ &+\frac{1}{2}\partial_\mu\sigma\,\partial^\mu\sigma - \frac{1}{2}m_\sigma^2\sigma^2 - \frac{1}{3}g_2\sigma^3 - \frac{1}{4}g_3\sigma^4\\ &-\frac{1}{4}W_{\mu\nu}W^{\mu\nu} + \frac{1}{2}m_\omega^2\omega_\mu\omega^\mu\\ &-\frac{1}{4}R^a_{\mu\nu}R^{a\mu\nu} + \frac{1}{2}m_\rho^2\rho^a_\mu\rho^{a\mu}\\ &+\sum_{l=e,\mu}\bar{\psi}_l(i\gamma_\mu\partial^\mu - m_l)\psi_l, \end{aligned} \tag{1}$$

which contains the contributions of baryons (n and p) and leptons (e and μ). $W^{\mu\nu}$ and $R^{a\mu\nu}$ are the antisymmetric field tensors for ω^μ and $\rho^{a\mu}$, respectively. The parameters in the Lagrangian are usually determined by fitting nuclear matter saturation properties and/or ground-state properties of finite nuclei.

To study the effect of symmetry energy slope L, we generate a series of parameter sets with a density-dependent isovector coupling based on the NL3 parametrization (referred to as NL3L). The parameters and saturation properties of the original NL3 model are listed in Tables I and II, respectively. In NL3L, the symmetry energy slope parameter is tuned to be $L = 30$–110 MeV at the saturation density, as listed in Table III. The uncertainty of L does not affect the saturation properties of nuclear matter, that the NL3L parameter sets have the same saturation properties as the original NL3 except with different values of L. The isovector coupling g_ρ in NL3L is taken to be density-dependent as in the DDRMF approach,

$$g_\rho(n_b) = g_\rho(n_0)\exp\Big[-a_\rho\Big(\frac{n_b}{n_0}-1\Big)\Big], \tag{2}$$

where n_0 is the saturation density. Through this way, the symmetry energy slope L can be tailored conveniently by adjusting a_ρ without affecting other saturation properties and leaving other parameters the same as the original ones. The density dependence of g_ρ contributes a rearrangement item for nucleons,

$$\Sigma_r = \frac{1}{2}\sum_{i=p,n}\frac{\partial g_\rho(n_b)}{\partial n_b}\tau_3 n_i\rho = -\frac{1}{2}a_\rho g_\rho(n_b)\frac{n_p-n_n}{n_0}\rho. \tag{3}$$

In a homogeneous matter, the meson field equations have the following form:

$$m_\sigma^2\sigma + g_2\sigma^2 + g_3\sigma^3 = -g_\sigma\big(n_p^s + n_n^s\big), \tag{4}$$

$$m_\omega^2\omega = g_\omega(n_p+n_n), \tag{5}$$

$$m_\rho^2\rho = \frac{g_\rho(n_b)}{2}(n_p-n_n), \tag{6}$$

where n_i^s and n_i represent the scalar and vector densities of the ith baryon ($i = n, p$), respectively. The equations of motion for nucleons give the standard relations between the densities and chemical potentials,

$$\mu_p = \sqrt{\big(k_F^p\big)^2 + M^{*2}} + g_\omega\omega + \Sigma_r + \frac{g_\rho(n_b)}{2}\rho, \tag{7}$$

$$\mu_n = \sqrt{\big(k_F^n\big)^2 + M^{*2}} + g_\omega\omega + \Sigma_r - \frac{g_\rho(n_b)}{2}\rho, \tag{8}$$

where $M^* = M + g_\sigma\sigma$ is the effective nucleon mass, and k_F^i is the Fermi momentum of species i, which is related to the vector density by $n_i = (k_F^i)^3/3\pi^2$. For neutron-star matter in β equilibrium, the chemical potentials satisfy the relations $\mu_p = \mu_n - \mu_e$ and $\mu_\mu = \mu_e$, where the chemical potentials of leptons are given by $\mu_l = \sqrt{(k_F^l)^2 + m_l^2}$.

In neutron-star matter, the total energy density and pressure are given by

$$\begin{aligned}\varepsilon = &\sum_{i=p,n}\frac{1}{\pi^2}\int_0^{k_F^i}\sqrt{k^2+M^{*2}}k^2dk\\ &+\frac{1}{2}m_\sigma^2\sigma^2 + \frac{1}{3}g_2\sigma^3 + \frac{1}{4}g_3\sigma^4 + \frac{1}{2}m_\omega^2\omega^2\\ &+\frac{1}{2}m_\rho^2\rho^2 + \varepsilon_l, \end{aligned} \tag{9}$$

$$\begin{aligned}P = &\sum_{i=p,n}\frac{1}{3\pi^2}\int_0^{k_F^i}\frac{1}{\sqrt{k^2+M^{*2}}}k^4dk\\ &-\frac{1}{2}m_\sigma^2\sigma^2 - \frac{1}{3}g_2\sigma^3 - \frac{1}{4}g_3\sigma^4 + \frac{1}{2}m_\omega^2\omega^2\\ &+\frac{1}{2}m_\rho^2\rho^2 + n_b\Sigma_r + P_l, \end{aligned} \tag{10}$$

where ε_l and P_l ($l = e, \mu$) are the energy density and the pressure from leptons, respectively. With given baryon number density n_b, the EOS can be derived by solving the meson field

TABLE III. Parameter a_ρ generated from the NL3 model for different slope L at saturation density n_0 without changing other saturation properties. The original NL3 model has $L = 118.5$ MeV.

L (MeV)	30.0	40.0	50.0	60.0	70.0	80.0	90.0	100.0	110.0	118.5
a_ρ	0.7537	0.6686	0.5835	0.4983	0.4132	0.3280	0.2429	0.1578	0.0726	0

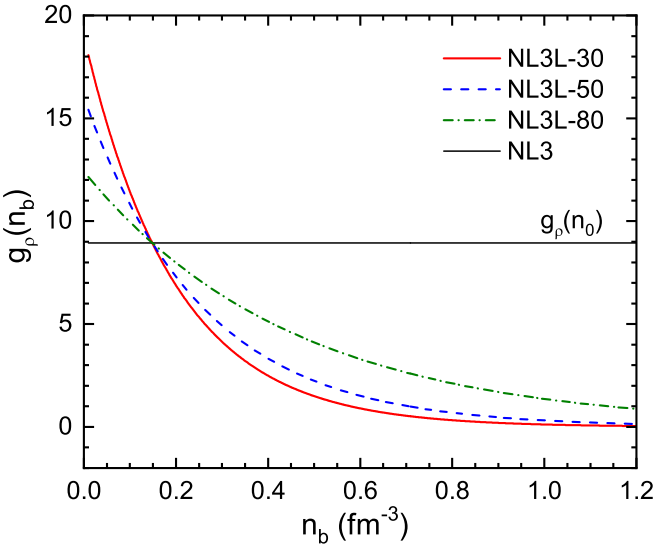

FIG. 1. Isovector coupling $g_\rho(n_b)$ as a function of the baryon number density n_b for different NL3L parameter sets. The horizontal line indicates the density-independent isovector coupling $g_\rho(n_0)$ in the original NL3 model.

equations under the conditions of β equilibrium and charge neutrality.

III. THE RESULTS AND DISCUSSION

In this section, we investigate the symmetry energy effect on the EOS and properties of neutron stars. It is well known that the symmetry energy slope L can significantly affect the neutron-star radius and tidal deformability. However, its value is still very uncertain and cannot be well constrained from current observations [39]. We apply the RMFL model to generate NL3L parameter sets with different values of L. In Fig. 1, we plot the density-dependent behavior of the isovector coupling $g_\rho(n_b)$ as a function of the baryon number density n_b. The original NL3 parameter set has fixed $g_\rho(n_b) = g_\rho(n_0)$. In the following discussions, we investigate the symmetry energy effect by comparing the results of $L = 30, 50, 80$ MeV (named as NL3L-30, NL3L-50, and NL3L-80), and the original NL3 parametrization with $L = 118.5$ MeV. It can be found that $g_\rho(n_b)$ decreases as the density n_b increases, and a smaller g_ρ results in smaller symmetry energy. At subnuclear densities ($n_b < n_0$), the coupling constant $g_\rho(n_b)$ is bigger than $g_\rho(n_0)$, while it becomes smaller at high densities. This trend can be easily understood from Eq. (2). Furthermore, a smaller L corresponds to a more rapid decrease of g_ρ.

We plot the symmetry energy S and the energy per nucleon E/A as a function of the baryon number density n_b in the left and right panels of Fig. 2. The results of NL3L-30, NL3L-50, NL3L-80, and the original NL3 parameter sets are shown. It is seen that the symmetry energy with a smaller L is lower (higher) than that with a larger L at $n_b > n_0$ ($n_b < n_0$), similar behavior is observed in Ref. [46]. The differences among NL3L-30, NL3L-50, and NL3L-80 are smaller than those with the original NL3. Especially, the symmetry energies of NL3L-30, NL3L-50, and NL3L-80 show a much slower increase than that of the original NL3 beyond two times saturation density. Different NL3L parametrizations have the same energy (E/A) for symmetry nuclear matter (SNM), since the isovector interaction vanishes in SNM [see Eq. (6)]. In contrast, E/A in pure neutron matter (PNM) shows a significant dependence on L. The L dependence of E/A in PNM is very similar to that of S, which can be understood from the relation $E/A(\text{PNM}) \approx E/A(\text{SNM}) + S$. Comparing with the constraints from isobaric analog states [84], relatively large symmetry energy at subnuclear density is obtained with a small L like NL3L-30. However, the results of S and E/A in PNM at 1–2n_0 are consistent with those obtained from Skyrme interactions [85], chiral effective field theory [86], and some stiff DDRMF models [41].

In Fig. 3, we show the EOSs with different L as a function of the baryon mass density ρ_b (left panel) and number density n_b (right panel), respectively. The green shaded area indicates the constraint by assuming the secondary component of GW190814 is a neutron star [4]. It is seen that the results of NL3L-30 and NL3L-50 are more consistent with the constraint than the original NL3 parametrization. Besides, these NL3L parametrizations could be better matched to the

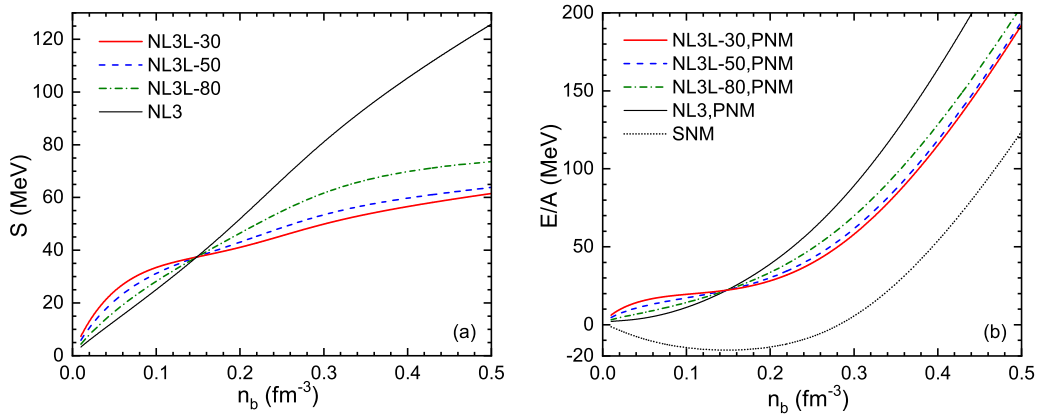

FIG. 2. Symmetry energy S (a) and energy per nucleon E/A in pure neutron matter (PNM) and symmetry nuclear matter (SNM) (b) as a function of the baryon number density n_b for different parameter sets. There is no difference in E/A of SNM for all parametrizations, whereas the results of S and E/A of PNM show different density dependence with the same value at saturation density n_0.

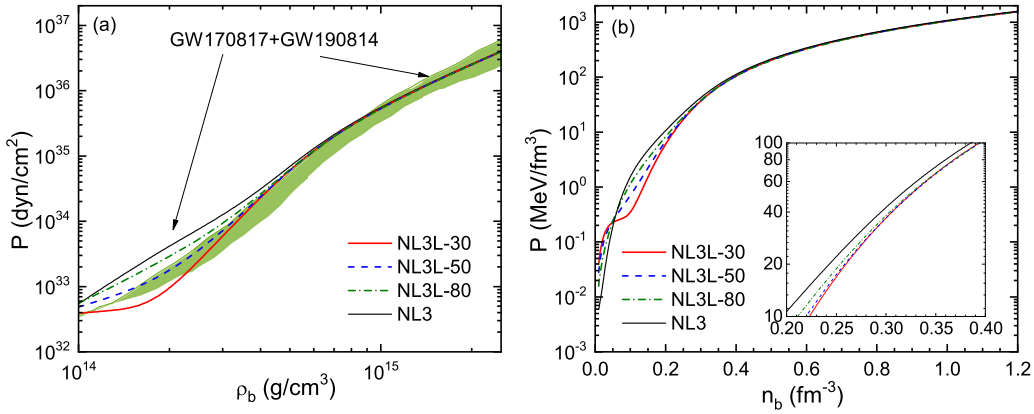

FIG. 3. Pressures as a function of the baryon mass density ρ_b (a) and number density n_b (b) obtained using different parameter sets. The green shaded area represents the joint constraints from GW170817 and GW190814 (assumed to be a NS-BH merger) [4].

green shaded area at high densities compared with the EOSs in Refs. [30,34]. From the right panel, we see that there are visible differences among different L lines at low densities ($n_b < 0.3$ fm^{-3}), while all NL3L parameter sets result in very similar EOSs at high densities. This behavior is related to the density dependence of g_ρ shown in Fig. 1. At low densities, the differences in g_ρ correspond to different isovector contributions, which yield different EOSs. However, g_ρ of all NL3L parametrizations decrease with increasing density and approach zero at high densities, so the differences caused by ρ meson tend to disappear. Considering the constraints shown in the left panel, it is clear that a stiff enough EOS like NL3L is helpful to support massive neutron star and a proper small L is favored at low density. To better understand the high-density EOS behavior, we show the proton fraction Y_p under β equilibrium as a function of the baryon number density n_b in Fig. 4. One can see that Y_p obtained in NL3L parametrizations with various L are different from each other at low densities, but they become very close at high densities. However, Y_p in the original NL3 model is obviously different from those of NL3L, since g_ρ has different behavior as shown in Fig. 1. The pressure is mainly contributed by nuclear Fermi energy and interaction. On one hand, at high densities, the contribution of isovector interaction to pressure decreases. On the other hand, the Y_p obtained by different L tends to be the same, which leads to close proton and neutron Fermi energies. Hence the pressures from NL3L are indistinguishable at high densities. The original NL3 model has different trends of Y_p and g_ρ from NL3L, which leads to a visible difference of pressure (see the insert of Fig. 3(b)).

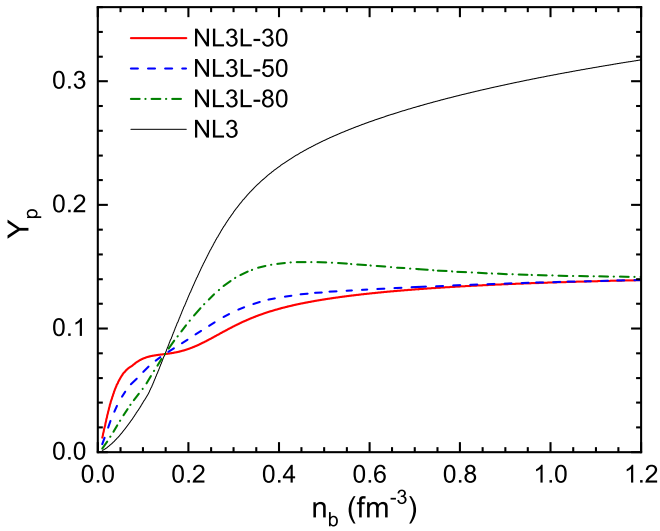

FIG. 4. Proton fraction Y_p in neutron-star matter as a function of the baryon number density n_b for different parameter sets.

To examine the effect of symmetry energy slope L on the properties of neutron stars, we solve the Toman-Oppenheimer-Volkoff (TOV) equations by using the NL3L parametrizations and the original NL3 model. The observed PSR J1614-2230, PSR J0348+0432, and PSR J0704+6620 suggest the neutron-star maximum mass $M_{\rm TOV}$ should be at least larger than 2 $M_\odot$. Using the EOS of neutron-star matter, the original NL3 parameter set predicts a maximum mass of 2.77 $M_\odot$. In Fig. 5, the mass-radius relation with different L is presented in panel (a), and the neutron-star mass as a function of the neutron-star central density n_c is shown in panel (b). Within the NL3 and NL3L models, the neutron-star maximum mass could be larger than 2.6 $M_\odot$, though with $L = 30$, 50, 80 MeV, there exists a tiny decrease of $M_{\rm TOV}$ (Table IV). The NL3L-30 and NL3L-50 parameter sets could satisfy the constraints from NICER [57,58] and the estimation of $R_{1.4} \leqslant 13.6$ km from GW170817 [29]. It is shown that a smaller L corresponds to a smaller radius, but this L dependence becomes much weaker for massive neutron stars. Besides, the L effect on the relation of the neutron-star central density n_c and mass is also small except at lower central densities. This is because L affects the EOSs at the

TABLE IV. Neutron star properties predicted by the NL3 and NL3L models.

Model	NL3L-30	NL3L-50	NL3L-80	NL3
$M_{\rm TOV}$ ($M_\odot$)	2.75	2.74	2.73	2.77
$R_{1.4}$ (km)	13.04	13.31	13.80	14.55
$\Lambda_{1.4}$	608.8	815.9	975.2	1242.4
n_c (fm^{-3})	0.689	0.690	0.693	0.680

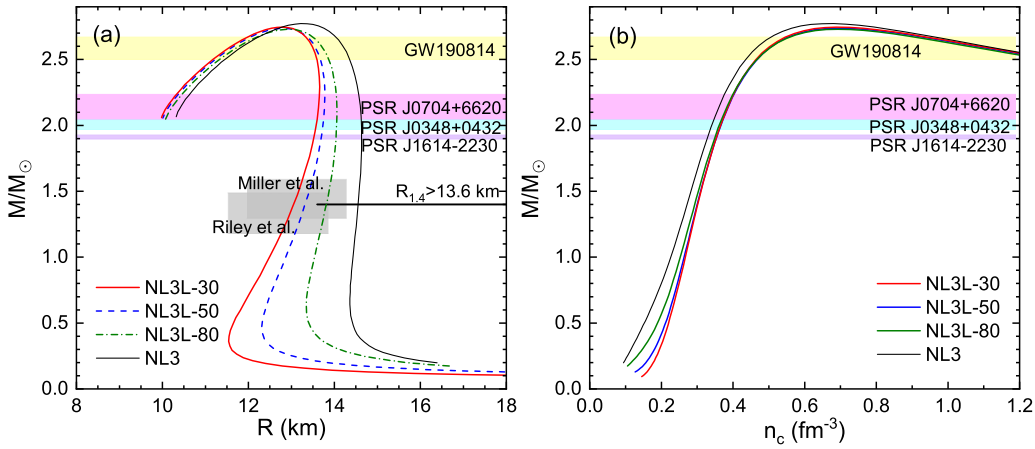

FIG. 5. Neutron-star masses as a function of the radius R (a) and the central density n_c (b) for different parameter sets. The colored bands indicate the mass measurements of PSR J1614-2230 [49–51], PSR J0348+0432 [52], and PSR J0740+6620 [5], while the mass constraint from GW190814 [4] is shown in yellow color. The grey shaded area represents the constraints from NICER [57,58]. The excluded region of $R_{1.4} > 13.6$ km inferred from GW170817 [29] is also indicated.

low-density region $n_b \leqslant 0.3$ fm^{-3} while EOSs keep almost the same at high density (see Fig. 3(b)). The maximum mass neutron star has a central density of $n_c \approx 0.7$ fm^{-3}. The tidal deformability as a function of the neutron-star mass is plotted in Fig. 6, and the details of massive neutron stars are shown in logarithmic coordinates in the upper right corner. The orange colored constraint $458 \leqslant \Lambda_{1.4} \leqslant 889$ [4] in the figure comes from a presupposition that the secondary component of GW190814 is a neutron star. It is shown that the results of NL3L-30 and NL3L-50 are consistent with this constraint. The results of $L \geqslant 50$ MeV are beyond the upper limit of $\Lambda_{1.4} \leqslant 800$ deduced from GW170817 [2]. However, even with the smallest L (NL3L-30), the resulting $\Lambda_{1.4}$ lies outside

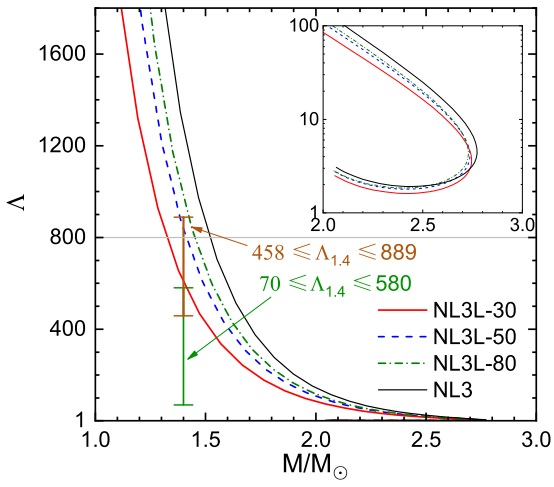

FIG. 6. Tidal deformability as a function of the neutron-star mass for different parameter sets. The constraint $70 \leqslant \Lambda_{1.4} \leqslant 580$ is inferred from the analysis of GW170817 [54], while $458 \leqslant \Lambda_{1.4} \leqslant 889$ is achieved based on the assumption that GW190814 is a NS-BH binary [4]. The horizontal line represents the upper limit of $\Lambda_{1.4} \leqslant 800$ deduced from GW170817 [2].

the constraint $70 \leqslant \Lambda_{1.4} \leqslant 580$ (green colored in Fig. 6) from the subsequent analysis of GW170817 [54].

IV. SUMMARY

In summary, motivated by the observation of the 2.6 $M_\odot$ object of GW190814, we have explored if such a massive object could be a neutron star. Since the lack of an electromagnetic counterpart to GW190814 and no tidal distortions observed from gravitational waveform, the secondary component of GW190814 may be a black hole or the heaviest neutron star ever observed. We applied the RMFL model with the NL3L parametrizations to describe the neutron-star matter. To study the effect of symmetry energy and its slope, we have employed a density-dependent coupling $g_\rho(n_b)$ as in the DDRMF approach.

Using a group of NL3L parameter sets, we have investigated the symmetry energy effect on the EOS and properties of neutron stars. It was found that a smaller L corresponds to smaller symmetry energy at $n_b > n_0$, which leads to lower pressure in neutron-star matter. However, at sufficiently high density the L dependence of EOSs tends to disappear due to rather small values of g_ρ. We found that these NL3L parametrizations provide EOSs that are stiff enough to support $M_{\rm TOV} > 2.6\,M_\odot$. The resulting EOSs of NL3L-30 and NL3L-50 lie roughly in the area constrained by assuming the secondary component of GW190814 is a neutron star. The neutron-star radii using NL3L-30, NL3L-50, and NL3L-80 are consistent with NICER constraints, while the results of NL3L-30 and NL3L-50 satisfy the constraints of $\Lambda_{1.4} = 616^{+273}_{-158}$ and $R_{1.4} = 12.9^{+0.8}_{-0.7}$ km [4] that correspond to GW190814 being a NS-BH binary. However, even with the smallest L (NL3L-30), we obtained $\Lambda_{1.4} = 608.8$ that is slightly larger than the constraint $70 \leqslant \Lambda_{1.4} \leqslant 580$ from GW170817. Since the maximum mass $M_{\rm TOV}$ is mainly determined by the high-density EOS, all of the NL3L parameter sets can support 2.6 $M_\odot$ neutron stars. Furthermore, a smaller L leads to smaller radii and tidal deformability of neutron stars, which can be compatible with current observations.

Although there are considerable uncertainties and model dependence in the present calculations, the possibility that the secondary component of GW190814 is a massive neutron star cannot be excluded. More precise measurement of tidal deformability for neutron stars by the gravitational wave detectors may help to constrain the EOS of neutron-star matter in the future.

ACKNOWLEDGMENTS

This work is supported by the National Key R&D Program of China (Grants No. 2018YFA0404703 and No. 2017YFA0402602), and the National Natural Science Foundation of China (Grants No. 11673002, No. U1531243, and No. 11805115).

[1] B. P. Abbott *et al.* (LIGO Scientific Collaboration and Virgo Collaboration), Phys. Rev. Lett. **116**, 061102 (2016).
[2] B. P. Abbott *et al.* (LIGO Scientific and Virgo Collaborations), Phys. Rev. Lett. **119**, 161101 (2017).
[3] B. P. Abbott *et al.* (LIGO Scientific and Virgo Collaborations), Astrophys. J. Lett. **900**, L13 (2020).
[4] R. Abbott *et al.* (LIGO Scientific and Virgo Collaborations), Astrophys. J. Lett. **896**, L44 (2020).
[5] H. T. Cromartie *et al.*, Nat. Astron. **4**, 72 (2020).
[6] X. H. Wu, S. Du, and R. X. Xu, Mon. Not. R. Astron. Soc. **499**, 4526 (2020).
[7] M. Zevin, M. Spera, Ch. P. L. Berry, and V. Kalogera, Astrophys. J. Lett. **899**, L1 (2020).
[8] M. Safarzadeh and A. Loeb, Astrophys. J. Lett. **899**, L15 (2020).
[9] R. Essick and P. Landry, Astrophys. J. **904**, 80 (2020).
[10] B. Biswas, R. Nandi, P. Char, S. Bose, and N. Stergioulas, Mon. Not. R. Astron. Soc. **505**, 1600 (2021).
[11] Y. Lim, A. Bhattacharya, J. W. Holt, and D. Pati, arXiv:2007.06526.
[12] M. Shibata, E. Zhou, K. Kiuchi, and S. Fujibayashi, Phys. Rev. D **100**, 023015 (2019).
[13] I. Tews, P. T. H. Pang, T. Dietrich, M. W. Coughlin, S. Antier, M. Bulla, J. Heinzel, and L. Issa, Astrophys. J. Lett. **908**, L1 (2021).
[14] A. Nathanail, E. R. Most, and L. Rezzolla, Astrophys. J. Lett. **908**, L28 (2021).
[15] V. Dexheimer, R. O. Gomes, T. Klähn, S. Han, and M. Salinas, Phys. Rev. C **103**, 025808 (2021).
[16] A. Kanakis-Pegios, P. S. Koliogiannis, and Ch. C. Moustakidis, Symmetry **13**, 183 (2021).
[17] E. R. Most, L. J. Papenfort, L. R. Weih, and L. Rezzolla, Mon. Not. R. Astron. Soc. **499**, L82 (2020).
[18] A. Tsokaros, M. Ruiz, and S. L. Shapiro, Astrophys. J. **905**, 48 (2020).
[19] T. Demircik, C. Ecker, and M. Järvinen, Astrophys. J. Lett. **907**, L37 (2021).
[20] N.-B. Zhang and B.-A. Li, Astrophys. J. **902**, 38 (2020).
[21] J. J. Li, A. Sedrakian, and F. Weber, Phys. Lett. B **810**, 135812 (2020).
[22] G. B. Cook, S. L. Shapiro, and S. A. Teukolsky, Astrophys. J. **424**, 823 (1994); **422**, 227 (1994).
[23] C. Breu and L. Rezzolla, Mon. Not. R. Astron. Soc. **459**, 646 (2016).
[24] J. W. T. Hessels, S. M. Ransom, I. H. Stairs, P. C. C. Freire, V. M. Kaspi, and F. Camilo, Science **311**, 1901 (2006).
[25] R. Essick, P. Landry, and D. E. Holz, Phys. Rev. D **101**, 063007 (2020).
[26] J. W. Moffat, arXiv:2008.04404.
[27] R. C. Nunes, J. G. Coelho, and J. C. N. de Araujo, Eur. Phys. J. C **80**, 1115 (2020).
[28] A. V. Astashenok, S. Capozziello, S. D. Odintsov, and V. K. Oikonomou, Phys. Lett. B **811**, 135910 (2020).
[29] E. Annala, T. Gorda, A. Kurkela, and A. Vuorinen, Phys. Rev. Lett. **120**, 172703 (2018).
[30] K. X. Huang, J. N. Hu, Y. Zhang, and H. Shen, Astrophys. J. **904**, 39 (2020).
[31] A. Sedrakian, F. Weber, and J.-J. Li, Phys. Rev. D **102**, 041301(R) (2020).
[32] D. A. Godzieba, D. Radice, and S. Bernuzzi, Astrophys. J. **908**, 122 (2021).
[33] F. J. Fattoyev, C. J. Horowitz, J. Piekarewicz, and B. Reed, Phys. Rev. C **102**, 065805 (2020).
[34] H. Tan, J. Noronha-Hostler, and N. Yunes, Phys. Rev. Lett. **125**, 261104 (2020).
[35] L. McLerran and S. Reddy, Phys. Rev. Lett. **122**, 122701 (2019).
[36] I. Bombaci, A. Drago, D. Logoteta, G. Pagliara, and I. Vidaña, Phys. Rev. Lett. **126**, 162702 (2021).
[37] Z. Roupas, G. Panotopoulos, and I. Lopes, Phys. Rev. D **103**, 083015 (2021).
[38] Z. Cao, L.-W. Chen, P.-C. Chu, and Y. Zhou, arXiv:2009.00942.
[39] M. Oertel, M. Hempel, T. Klähn, and S. Typel, Rev. Mod. Phys. **89**, 015007 (2017).
[40] F. J. Fattoyev, J. Piekarewicz, and C. J. Horowitz, Phys. Rev. Lett. **120**, 172702 (2018).
[41] J. N. Hu, S. S. Bao, Y. Zhang, K. Nakazato, K. Sumiyoshi, and H. Shen, Prog. Theor. Exp. Phys. **2020**, 043D01 (2020).
[42] M. Centelles, X. Roca-Maza, X. Vinas, and M. Warda, Phys. Rev. Lett. **102**, 122502 (2009).
[43] A. W. Steiner and S. Gandolfi, Phys. Rev. Lett. **108**, 081102 (2012).
[44] J. M. Lattimer and Y. Lim, Astrophys. J. **771**, 51 (2013).
[45] I. Tews, J. M. Lattimer, A. Ohnishi, and E. E. Kolomeitsev, Astrophys. J. **848**, 105 (2017).
[46] S. S. Bao, J. N. Hu, Z. W. Zhang, and H. Shen, Phys. Rev. C **90**, 045802 (2014).
[47] A. Drago, A. Lavagno, and G. Pagliara, Phys. Rev. D **89**, 043014 (2014).
[48] W. M. Spinella, A systematic investigation of exotic matter in neutron stars, Ph.D. thesis, Claremont Graduate University & San Diego State University, 2017.
[49] P. B. Demorest, T. Pennucci, S. M. Ranson, M. S. E. Roberts, and J. W. T. Hessels, Nature (London) **467**, 1081 (2010).
[50] E. Fonseca *et al.*, Astrophys. J. **832**, 167 (2016).
[51] Z. Arzoumanian *et al.*, Astrophys. J. Suppl. **235**, 37 (2018).
[52] J. Antoniadis, P. C. C. Freire, N. Wex *et al.*, Science **340**, 1233232 (2013).

[53] M. Linares, T. Shahbaz, and J. Casares, Astrophys. J. **859**, 54 (2018).
[54] B. P. Abbott *et al.* (LIGO Scientific and Virgo Collaborations), Phys. Rev. Lett. **121**, 161101 (2018).
[55] E. R. Most, L. R. Weih, L. Rezzolla, and J. Schaffner-Bielich, Phys. Rev. Lett. **120**, 261103 (2018).
[56] G. Raaijmakers *et al.*, Astrophys. J. Lett. **887**, L22 (2019).
[57] M. C. Miller *et al.*, Astrophys. J. Lett. **887**, L24 (2019).
[58] T. E. Riley *et al.*, Astrophys. J. Lett. **887**, L21 (2019).
[59] B. Margalit and B. D. Metzger, Astrophys. J. Lett. **850**, L19 (2017).
[60] L. Rezzolla, E. R. Most, and L. R. Weih, Astrophys. J. Lett. **852**, L25 (2018).
[61] M. Ruiz, S. L. Shapiro, and A. Tsokaros, Phys. Rev. D **97**, 021501(R) (2018).
[62] B. P. Abbott *et al.* (LIGO Scientific and Virgo Collaborations), Classical and Quantum Gravity **37**, 045006 (2020).
[63] S. Weinberg, Physica A **96**, 327 (1979).
[64] E. Epelbaum, H.-W. Hammer, and Ulf-G. Meißner, Rev. Mod. Phys. **81**, 1773 (2009).
[65] R. Machleidt and D. R. Entem, Phys. Rep. **503**, 1 (2011).
[66] J. W. Holt and N. Kaiser, Phys. Rev. C **95**, 034326 (2017).
[67] J. W. Holt and Y. Lim, Phys. Lett. B **784**, 77 (2018).
[68] D. Adhikari *et al.* (PREX Collaboration), Phys. Rev. Lett. **126**, 172502 (2021).
[69] B. T. Reed, F. J. Fattoyev, C. J. Horowitz, and J. Piekarewicz, Phys. Rev. Lett. **126**, 172503 (2021).
[70] R. Essick, I. Tews, P. Landry, and A. Schwenk, arXiv:2102.10074.
[71] G. A. Lalazissis, J. König, and P. Ring, Phys. Rev. C **55**, 540 (1997).
[72] Phys. Rev. A-Editors, Phys. Rev. A **83**, 040001 (2011).
[73] J. Erler, C. J. Horowitz, W. Nazarewicz, M. Rafalski, and P.-G. Reinhard, Phys. Rev. C **87**, 044320 (2013).
[74] W.-C. Chen and J. Piekarewicz, Phys. Rev. C **90**, 044305 (2014).
[75] J. Dobaczewski, W. Nazarewicz, and P.-G. Reinhard, J. Phys. G **41**, 074001 (2014).
[76] J. Piekarewicz, W.-C. Chen, and F. J. Fattoyev, J. Phys. G **42**, 034018 (2015).
[77] W.-C. Chen and J. Piekarewicz, Phys. Lett. B **748**, 284 (2015).
[78] B. D. Carlsson, Phys. Rev. C **95**, 034002 (2017).
[79] J. Yang and J. Piekarewicz, Annu. Rev. Nucl. Part. Sci. **70**, 21 (2020).
[80] W.-C. Chen and J. Piekarewicz, Phys. Rev. C **102**, 042801(R) (2020).
[81] C. Ishizuka, A. Ohnishi, K. Tsubakihara, K. Sumiyoshi, and S. Yamada, J. Phys. G **35**, 085201 (2008).
[82] X. H. Wu and H. Shen, Phys. Rev. C **96**, 025802 (2017).
[83] X. H. Wu, A. Ohnishi, and H. Shen, Phys. Rev. C **98**, 065801 (2018).
[84] P. Danielewicz and J. Lee, Nucl. Phys. A **922**, 1 (2014).
[85] M. Dutra, O. Lourenço, J. S. Sá Martins, A. Delfino, J. R. Stone, and P. D. Stevenson, Phys. Rev. C **85**, 035201 (2012).
[86] D. Lonardoni, I. Tews, S. Gandolfi, and J. Carlson, Phys. Rev. Research **2**, 022033(R) (2020).